Analytical and Bioanalytical Chemistry
https://doi.org/10.1007/s00216-023-05055-1

RESEARCH PAPER

Analysis and experimental assessment of an optimized SERS substrate used to detect thiabendazole in apples with high sensitivity

Xiaodong Li[1,2] · Yanyan Zhang[1,2] · Muhammad Awais[1,2] · Hao Zhang[1,2] · Syed Muhammad Zaigham Abbas Naqvi[1,2] · Linze Li[1,2] · Yani Xiong[1,2] · Jiandong Hu[1,2,3]

Received: 13 October 2023 / Revised: 13 November 2023 / Accepted: 13 November 2023

Abstract

Pesticides that linger in the environment and ecosystems for an extended period can cause severe and dangerous health problems in humans. To detect pesticides in foods, the development of high-sensitivity and quick screening technologies was required. This research investigated the performance of Au@Ag NPs with varying thicknesses of the silver shell for detecting trace quantities of thiabendazole (TBZ) in apples using surface-enhanced Raman spectroscopy (SERS). The Au@Ag NPs were synthesized by coating 32 nm gold seeds with different thicknesses of silver shell ranging from 2.4 to 8.7 nm, achieved by adjusting the incorporation of $AgNO_3$ and ascorbic acid. The optimized Au@Ag NPs with a 7.3 nm silver shell demonstrated outstanding SERS activity, high sensitivity, and a detection limit of 0.05 μg/mL for TBZ. The R^2 values, representing the goodness of fit, were found to be 0.990 and 0.986 for standard and real TBZ samples, respectively, indicating a strong correlation between the measured signal and the TBZ concentration. The recovery analysis showed a reliable and accurate detection capability (96 to 105%), suggesting good reliability and accuracy of the SERS-based detection using the optimal Au@Ag NPs. Overall, this research highlights the potential of SERS with optimal Au@Ag NPs for rapid and effective monitoring of pesticides in the food industry.

Keywords Silver shell · Ag@Au NPs · Thiabendazole · Surface-enhanced Raman spectroscopy (SERS) · Apple

Introduction

Chemical pesticides have long been used in agricultural products to manage and eradicate pests and insects that transmit illnesses to plants or crops and cause harm to seeds during germination, growth, harvesting, and storage [1]. Because pesticides linger in the environment and ecosystems for extended periods and eventually penetrate food chains, their presence in fruit, vegetables, food items, and water sources can have severe and hazardous health impacts on humans [2]. Reproductive issues, neurotoxicity, liver damage, and developmental and physiological alterations in the organism are all examples of these disorders [3]. Given the persistently damaging impacts of pesticides on human health, it is imperative to develop and exploit technologies for screening and monitoring chemical pesticide residues as soon as possible.

Several laboratory analysis approaches based on classic pesticide detection technologies have been reported. High-performance liquid chromatography (HPLC) [4], liquid chromatography-mass spectrometry (LC-MS) [5], gas chromatography (GC) [6], capillary electrophoresis (CE) [7], and gas chromatography-mass spectrometry (GC-MS) [8] are examples of these technologies. All of these analysis approaches exhibited high sensitivity, strong repeatability, and outstanding selectivity, but were too expensive to use in laboratories due to pricey apparatus and sophisticated processing limits. Among the different pesticide-sensor technologies, optical sensor–based techniques are more important than others. Recent important developments in optical sensing research, such as infrared spectroscopy [9], UV-Vis spectroscopy [10], fluorescence spectroscopy [11], and surface-enhanced Raman spectroscopy (SERS) [12],

✉ Jiandong Hu
jdhu@henau.edu.cn

1 College of Mechanical and Electrical Engineering, Henan Agricultural University, Zhengzhou 450002, China

2 Henan International Joint Laboratory of Laser Technology in Agricultural Sciences, Zhengzhou 450002, China

3 State Key Laboratory of Wheat and Maize Crop Science, Zhengzhou 450002, China

Published online: 25 November 2023

have enabled quick pesticide monitoring in agricultural products. Optical sensing technology is distinguished by its resistance to electromagnetic interference, great selectivity, and high sensitivity at high temperatures and pressures [13]. Furthermore, when compared to other optical sensing technologies, SERS is extremely useful for practical and real-world applications.

SERS is a combination of Raman spectroscopy and nanotechnology that reveals fingerprint information of analytes quickly, sensitively, and without water interference [14]. Meanwhile, Raman scattering from molecules absorbed near noble metal nanoparticles can be greatly enhanced, resulting in exceptional amplification factors of up to 10^{14} at the single molecule level [15]. As a result of the discovery of extremely effective substrates, SERS-based sensors have been extensively studied for monitoring low-concentration analytes including pesticides [16], fungi [17], antibiotics [18], hormones [19], and viruses [20]. The sensitivity of SERS is critical for detecting genuine samples in food applications as the substrate improves. The substrate, core-shell nanostructure, has the benefit of excellent signal enhancement and easy synthesis using low-cost materials, particularly Au@Ag bimetal substrate, which has been widely used to assess pesticide residue in the food field [21]. Although, according to the SERS enhancement process, the "Hot spot" has traditionally been considered the main contributor to the significant enhancement of the Raman signal in the nanogap, different perspectives regard the thickness of the shell to be the most important contributor to the signal amplification [22]. Researchers are increasingly focused on core-shell nanostructures rather than just increasing the number of "Hot spots." As a result, it is critical to investigate the proper thickness of the shells.

Thiabendazole (TBZ), which can be used to treat fungal illnesses and has preventive therapeutic properties, is also often used to keep fruits and vegetables fresh [23]. In China's national food safety standards, the maximum residue limits of thiram in fruits and vegetables range from 0.05 to 10 mg/kg [24]. But its trace residues not only pollute food but also adversely impair the ecological environment and endanger human health [25]. As a result, TBZ pesticide pollution has raised concerns. Au@Ag bimetallic nanostructures are currently being used as SERS sensor substrates to detect and monitor TBZ in food safety. Nisar et al. used 2-mercaptoethanol, a novel improved substrate, to change the surface of Au@Ag nanoparticles. The detection of TBZ in apple puree was achieved with a LOD of roughly 0.0064 μg/mL and a high R^2 of 0.9968 [26]. Zou et al. manufactured varied sizes of Au@Ag nanorods as $AgNO_3$ concentration increased and created a fitting equation for three Raman peaks at varying TBZ concentrations in apple or peach juice samples. As a result, the optical R^2 was 0.99888 and 0.99884, respectively, and the LOD in real-world tests was 0.032 μg/mL and 0.034 μg/mL [27]. While the surface improvement of Au@Ag nanoparticles can result in excellent detection performance, it is important to consider the influence of the shell structure on the substrate. In contrast to the intricate synthesis process of Au@Ag nanorods, the preparation of spherical Au@Ag nanoparticles is straightforward, and they offer advantages such as extended storage time and enhanced detection capabilities. Consequently, researchers are more likely to favor their usage, and their practical applicability is significantly enhanced. However, there has been a lack of research investigating the optimal thickness of the Ag shell for detecting TBZ using Au@Ag nanoparticles in real-world materials.

In this study, the effect of core-shell thickness on the SERS response of Au@Ag nanoparticles (Au@Ag NPs) was examined and employed for the quantitative detection of TBZ residues in standard solutions and apple juice samples. To begin, as nuclei, spherical gold nanoparticles were manufactured, and the silver shell thickness of Au@Ag NPs was adjusted by varying the addition of silver nitrate core ascorbic acid. The Au@Ag NPs with different shell thicknesses were characterized and analyzed using UV-Vis spectroscopy, TEM, and XDR, respectively. The SERS response of R6G with Au@Ag NPs was utilized to determine the appropriate silver shell thickness, allowing the Au@Ag NPs to benefit from both silver and gold nanostructures. Finally, TBZ samples were generated in apple juice using the standard addition procedure, and the samples were directly combined with clean silicon wafers, dried, and quantitatively analyzed by SERS. This method not only provides a simple, inexpensive, and optimal SERS substrate for the SERS detection of TBZ but also has the potential for rapid analysis of other pesticide residues in food.

Materials and methods

Materials and instruments

All of the chemicals used in the studies were of analytical grade. Aladdin Reagents Co., Ltd (Shanghai, China) provided the gold chloride trihydrate ($HAuCl_4$), sodium citrate ($C_6H_5O_7Na_3$), silver nitrate ($AgNO_3$), ascorbic acid (AA, $C_6H_8O_6$), and thiabendazole. Sigma-Aldrich (USA) provided the Rhodamine 6 G (R6G, $C_{28}H_{30}N_2O_3$) and polyethylene glycol sorbitan monolaurate (Tween20). Sinopharm Chemical Reagent Co. supplied the methanol (CH_3OH). Apples were obtained from local supermarkets in Zhengzhou, China. All solution preparations were done with ultra-pure water, and any necessary analysis was done. The beakers and magnetic beads used in this investigation to manufacture precious metal nanoparticles were properly washed and dried after being soaked in aqua regia [HCl:HNO_3 = 3:1 (v/v)].

UV-Vis spectroscopy of gold nanoparticles and Au@Ag NPs was recorded in the wavelength range of 300–700 nm using UV-Vis spectroscopy (Nanjing Filer Instruments Co., Ltd., Nanjing, China). Centrifuges were utilized to extract contaminants from nanoparticles and solutions (Hunan Xiangyi Centrifuge Instrument Co., Ltd.). Before centrifugation, all tubes were washed with 0.05% TW20 solution to prevent nanoparticle adsorption on the tubes. Transmission electron microscopy (TEM, JEOL JEM-1400 Plus, Tokyo, Japan) was used to determine the morphology and size of gold nanoparticles and Au@Ag NPs. An energy spectrometer (EDS, Hitachi, Japan) was used to analyze the elements of Au@Ag NPs. A confocal Raman microscope system (Pioneer Technology Co., Ltd., Beijing, China) was used to capture the SERS signal.

Synthesis of core-shell Au@Ag NPs

The seed-mediated approach was used to create Au@Ag NPs [28]. Gold nanoparticles (32 nm) were created by boiling 950 µL of 0.5% chloroauric acid and 60 mL of ultrapure water, then adding 600 µL of 1% sodium citrate and heating for 6 min until the solution turned purple. The precipitated gold nanoparticles were disseminated in water after centrifugation for continued production of Au@Ag NPs. To make them, 3 mL of the gold nanoparticle solution was mixed with 150 µL of 10 mM AA and 150 µL of 10 mM $AgNO_3$ and agitated for 6 min until the solution turned orange. The amount of AA and $AgNO_3$ supplied (60–210 µL) was varied to produce Au@Ag NPs with variable silver shell thicknesses.

Preparation of TBZ sample

In this investigation, a stock solution of 100 µg/mL TBZ was produced in methanol, then diluted with ultrapure water and weighed at various concentrations (0.1, 0.5, 5, 10, 20 µg/mL). The TBZ in apple juice samples was prepared for the previously reported dependable standard addition procedure [29]. To make apple juice, apples were washed, cored, peeled, and filtered. Magnesium sulfate and sodium acetate were added to 3 mL of the prepared apple juice tube, followed by 1 mL of TBZ solution at various concentrations. The tubes were then centrifuged at 8000 rpm for 10 min and the supernatant was collected for Raman spectroscopy.

Surface-enhanced Raman detection and spectral processing

The R6G is a Raman probe molecule that was developed to validate the SERS-enhanced performance and repeatability of synthetic Au@Ag NPs. In each experiment, the obtained R6G, TBZ standard solution, or TBZ solution in the juice was mixed directly with an equal amount of synthesized Au@Ag NPs, and after washing with acetone, ethanol, and ultrapure water, single crystal silicon as a solid substrate (1 cm × 1 cm) was selected, and 2 µL of the mixture was dropped onto the surface of the silicon substrate to form droplets for Raman testing. The sample was pre-calibrated using silicon wafers before testing to ensure accurate spectra for experimental detection; the laser was focused using a 10 objective with an integration time of 5 s, and Raman spectra in the wavelength range of 600~1800 cm^{-1} were acquired with a Raman spectrometer, with the instrument parameters remaining constant throughout the experiment.

Selectivity experiment

To assess the selectivity of the Au@Ag NPs substrates for detecting thiabendazole, four commonly used pesticides (trichlorfon, thiram, chlorpyrifos, and dimethoate) were utilized as interference controls. The SERS spectra of the four insecticides were obtained under the given detection settings.

Data analysis

Because the original SRES spectra typically consisted of Raman signals mixed with background autofluorescence signals, it was essential to develop methods for extracting the pure Raman signals from the original data. To accomplish this, the Vancouver Raman Algorithm software was employed to process the raw Raman spectra and eliminate the background signal before obtaining the Raman spectral data.

Furthermore, linear fit curves for the association between Raman intensity at characteristic peak and target molecule concentration of TBZ standard solution and real juice sample have been produced. R^2, which was likewise derived by the concentration of real juice samples and recovery testing, was used to determine the trained accuracy of the above two linear curves. Furthermore, the relative standard deviation (RSD) was calculated by determining the average Raman intensity at feature peaks and the corresponding standard deviation.

Results and discussion

Fabrication and growth mechanism of Au@Ag NPs

Figure 1 shows the schematic representation of analysis and experimental assessment of Au@Ag NPs substrate used to detect thiabendazole in apples. These nanoparticles are created in two steps: first, Au NPs are created using the sodium citrate reduction procedure, and then

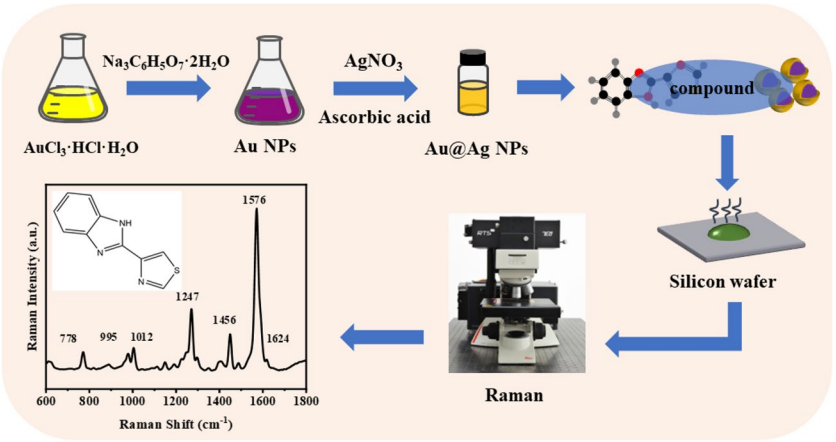

Fig. 1 Schematic representation of the analytical and experimental evaluation of optimized Au@Ag NPs for the detection of thiabendazole in apples

varied thicknesses of Ag shells are created with the controlled addition of AA and $AgNO_3$. Au@Ag NPs have the potential to improve the sensitivity of SERS detection by leveraging the unique features of both gold and silver. The nanoparticles are mixed with varied doses of TBZ before being drop-cast onto a silicon wafer and cured at room temperature for direct Raman spectroscopic measurement.

The characterization of shell-controlled Au@Ag NPs and gold nanoparticles

Nanoparticles are widely characterized using TEM and UV-Vis spectroscopy, which provide useful information on their size, shape, and optical properties. The TEM picture (Fig. 2a) and UV-Vis spectroscopy (Fig. 2b) of gold

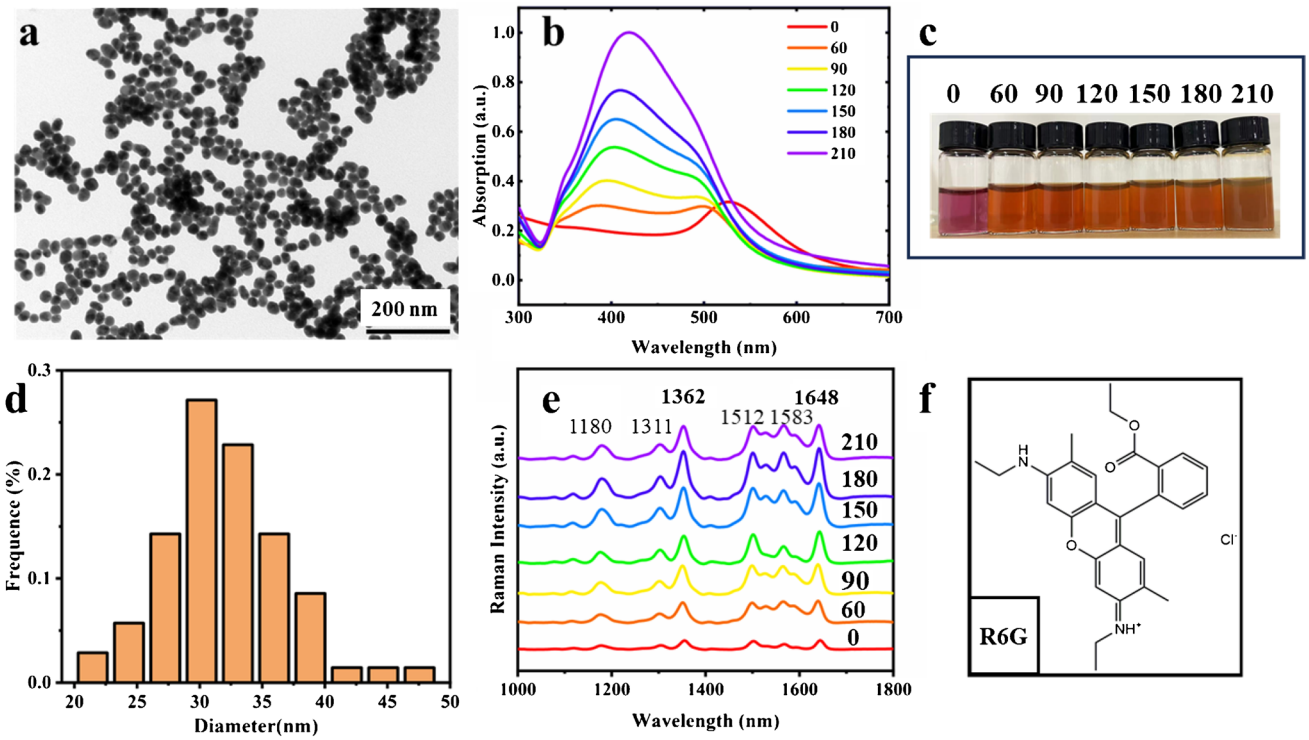

Fig. 2 The TEM image (**a**) of gold nanoparticles. Addition of 0, 60, 90, 120, 150, 180, and 210 µL of $AgNO_3$ to the synthesized Au@Ag NPs UV-Vis absorption spectroscopy (**b**) and solution picture (**c**). The particle size distribution of gold nanoparticles (**d**), SERS spectra of 10^{-5} M R6G adsorbed on Au@Ag NPs with different Ag shell thicknesses (**e**), and molecular structure of R6G (**f**)

nanoparticles are shown in Fig. 2. The TEM image shows that the gold nanoparticles have a spherical and homogeneous shape, with an average diameter of about 32 nm (Fig. 2d). Meanwhile, the gold nanoparticles' UV-Vis spectroscopy exhibits a small peak centered at 531 nm, which is attributable to surface plasmon resonance (SPR). These findings demonstrate that the effective synthesis of gold nanoparticles can be used as a starting point for the production of Au@Ag NPs.

Bimetallic nanoparticles with a silver shell on a gold core can be manufactured utilizing the seed-mediated approach to attain the optimum plasmonic characteristics. The thickness of the silver shell can be accurately regulated by changing the amount of AA and $AgNO_3$ injected, resulting in Au@Ag NPs with tailored optical and catalytic capabilities. The hue of Au@Ag NPs solution changes in Fig. 2c as different AA and $AgNO_3$ volumes are added. The solution color changes from purplish red to orange-yellow after adding $AgNO_3$, showing that silver is deposited on the surface of gold nanoparticles via $AgNO_3$ reduction by AA. UV-Vis absorption curves (Fig. 2b) reveal a new wavelength correlating to the Ag shell's SPR. The wavelengths of the gold and silver plasmon resonances of the Au@Ag colloidal sample produced using 60 µL $AgNO_3$ were 501 and 385 nm, respectively. The gold SPR peak decreased rapidly and was entirely shielded as the volume of $AgNO_3$ rose; however, the silver shell gradually stabilized with a slight red shift from 385 to 418 nm, indicating an increase in the thickness of the silver shell. It has been observed that incident light can only penetrate a specific thickness of the silver shell, and it is possible that after the silver shell reaches 7.3 nm, the incident light becomes difficult to excite the electrons in the gold nanoparticles. Furthermore, the thickness of the silver shell influences the SERS response. The SERS of R6G (Fig. 2f) using Au@Ag NPs revealed five unique peaks in the 1000–1800 nm range (Fig. 2e), with separate peaks at 1181 cm^{-1} for inward bending in the C-H plane and 1311, 1362, 1512, and 1648 cm^{-1} for the carbon skeleton stretching mode [15]. With the addition of $AgNO_3$ from 60 to 180 µL, the SERS intensity of R6G at the distinctive peaks 1362 and 1512 cm^{-1} steadily rose; however, the enhancement of SERS intensity slowed with additional increases in silver shell thickness (8.7 nm). However, even with 210 µL $AgNO_3$, the SERS reaction was still greater than in samples with 0 µL $AgNO_3$. Figure S1 shows the same result for different silver shells of Au@Ag adsorbing the same concentration of TBZ. Nonetheless, the colloidal color deepened to orange-yellow, and the UV-Vis spectroscopy band expanded, indicating agglomeration of the synthesized Au@Ag colloidal, which lowered the stability of the SERS enhancement

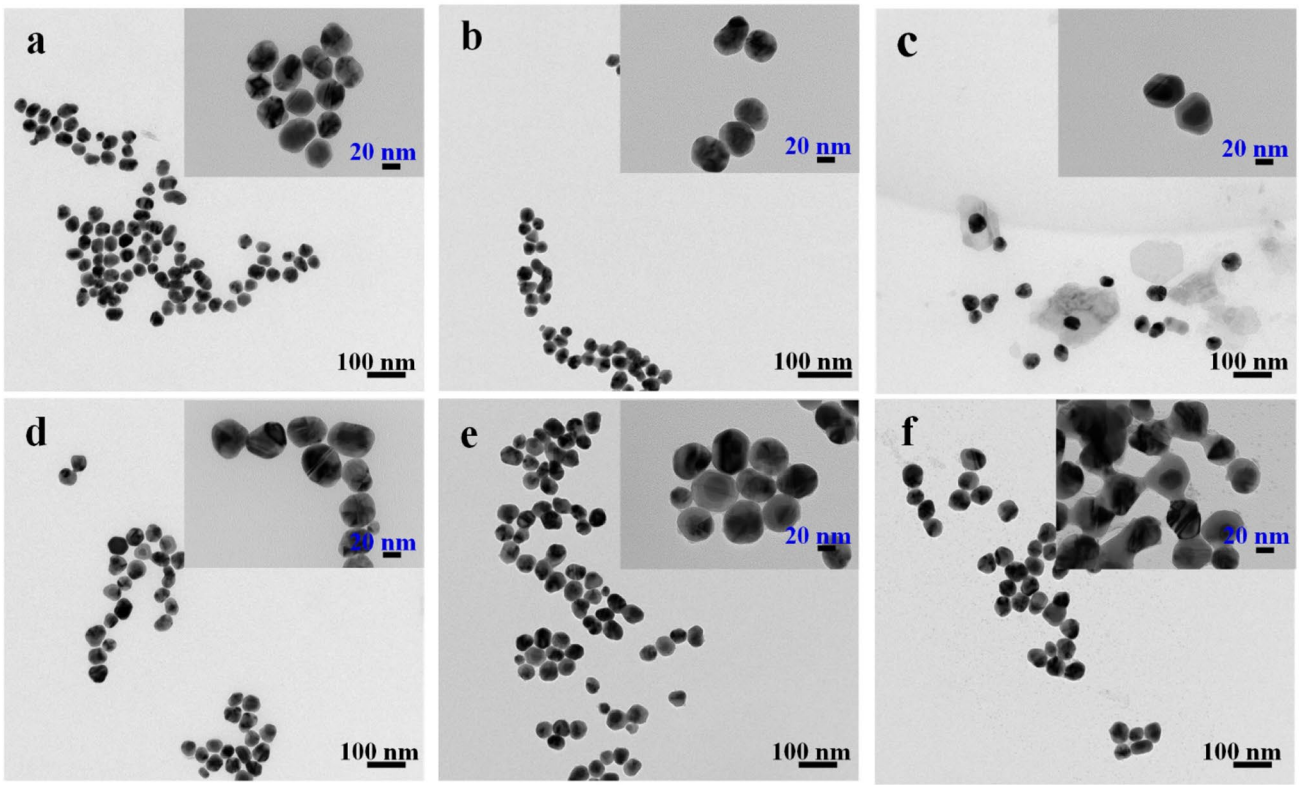

Fig. 3 The TEM images of Au@Ag NPs with average particle sizes of 2.4 (**a**), 3.9 (**b**), 5.2 (**c**), 6.3 (**d**), 7.3 (**e**), and 8.7 (**f**) nm, respectively

due to the silver shell rule on the surface of gold. The thickness of the silver shells in the six Au@Ag NPs (Fig. 3) was 2.4, 3.9, 5.2, 6.3, 7.3, and 8.7 nm, respectively. The synthesized Au@Ag NPs were characterized using HAADF-SEM to further validate the Au@Ag structure, and pictures of Au@Ag NPs with an Ag shell (gray filed) and Au core (white filed) are presented in Fig. 4c. As shown in Fig. 4(b, d, e, f), the energy spectrum revealed the existence of both Au and Ag components, confirming the successful preparation of Au@Ag NPs.

As a result, by varying the amounts of $AgNO_3$ and AA, the shape of the Au@Ag NPs and the thickness of the silver shells may be efficiently regulated. When the thickness of the silver shell deposited on the surface of gold nanoparticles surpasses 8.7 nm, the thickness of the silver shell deposited on the surface of gold nanoparticles becomes too big, resulting in uneven Au@Ag NPs and nanoparticle aggregation and sinking. In this study, Au@Ag NPs with a 32-nm gold core and 7.3-nm silver shell thickness were employed as the SERS enhancement substrate for subsequent studies to achieve an outstanding and stable SERS response.

Au@Ag NPs with enhanced SERS performance, reproducibility, and repeatability

The SERS substrate's SERS enhancement performance has a direct impact on its applicability in practical experiments. SERS signals from varying concentrations of R6G were collected to study the enhanced performance of Au@Ag NPs. The SERS spectra of R6G in Au@Ag NPs were recorded at concentrations of 10^{-8}, 10^{-9}, 10^{-10}, 10^{-11}, and 10^{-12} M, as shown in Fig. 5a. With decreasing concentration, the SERS of R6G signal intensity dropped. The SERS signal remains detectable even when the concentration of R6G is reduced to 10^{-10}~10^{-12}, and the surface Au@Ag NPs exhibit outstanding SERS amplification characteristics. The good linearity of SERS intensity at 1648 cm^{-1} vs logarithmic concentration for varied concentrations of R6G (Fig. 5b), $y = 1232.630x + 15518.265$, $R^2 = 0.998$. This also highlights the SERS base's better performance and prospective quantitative analysis capability.

The reliability and reproducibility of SERS substrates are critical in practical applications. The same concentration of R6G was detected repeatedly to test the bases' repeatability. The RSD of 9.37% for the repeated detection of 30 SERS spectra of R6G and its spectrum at 1648 cm^{-1} is shown in Fig. 5c and g, indicating that the base's repeatability is well established with no substantial deviation.

Long-term storage of nanoparticles colloidal may affect stability and reproducibility in SERS detection. The repeatability of Au@Ag colloidal is assessed in this work. The Au@Ag NPs were kept at −4 °C for 10 days before collecting the R6G SERS signal for 10 days (Fig. 5h and f). The SERS performance of Au@Ag NPs held for 10 days did not noticeably degrade, with an RSD of 14.09%. The reproducibility of new or existing SERS designs used for quantitative tests is usually acknowledged to have a point-to-point or substrate-to-substrate RSD of less than 20%. Notably, the Au@Ag NPs have superior repeatability. Furthermore,

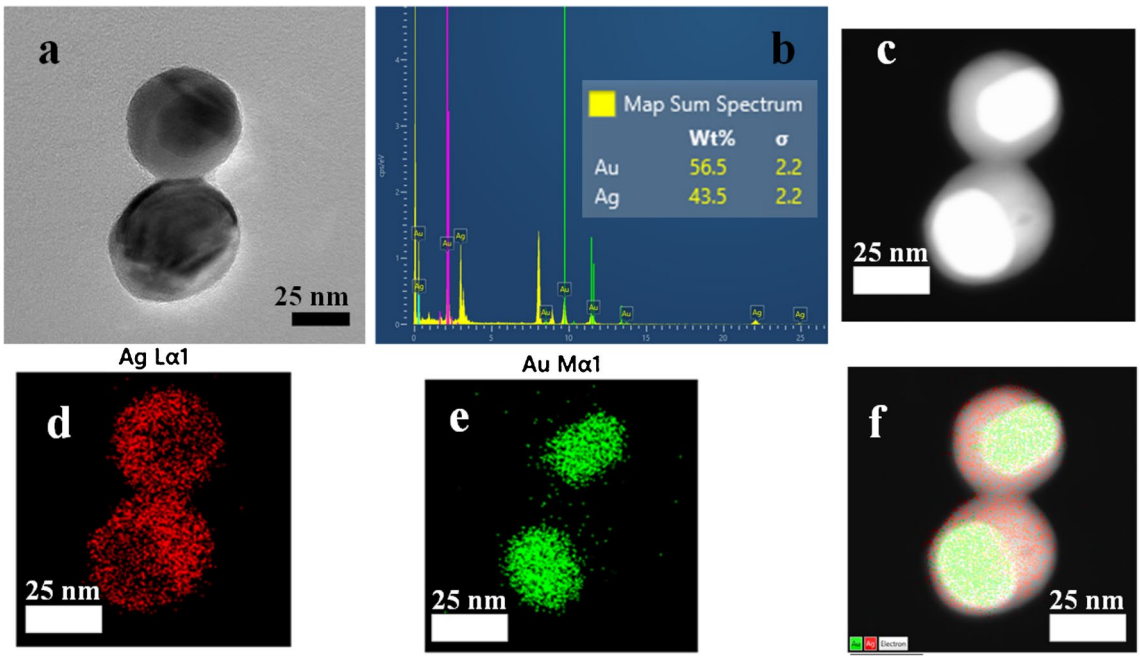

Fig. 4 The TEM image (**a**) and the existence of silver and gold in the EDS pattern confirmed the elemental composition of Au@Ag nanoparticle (**b**); HAADF-SEM image (**c**) of Au@Ag NPs; and EDS mapping of gold, silver, and Au@Ag (**d**, **e**, and **f**)

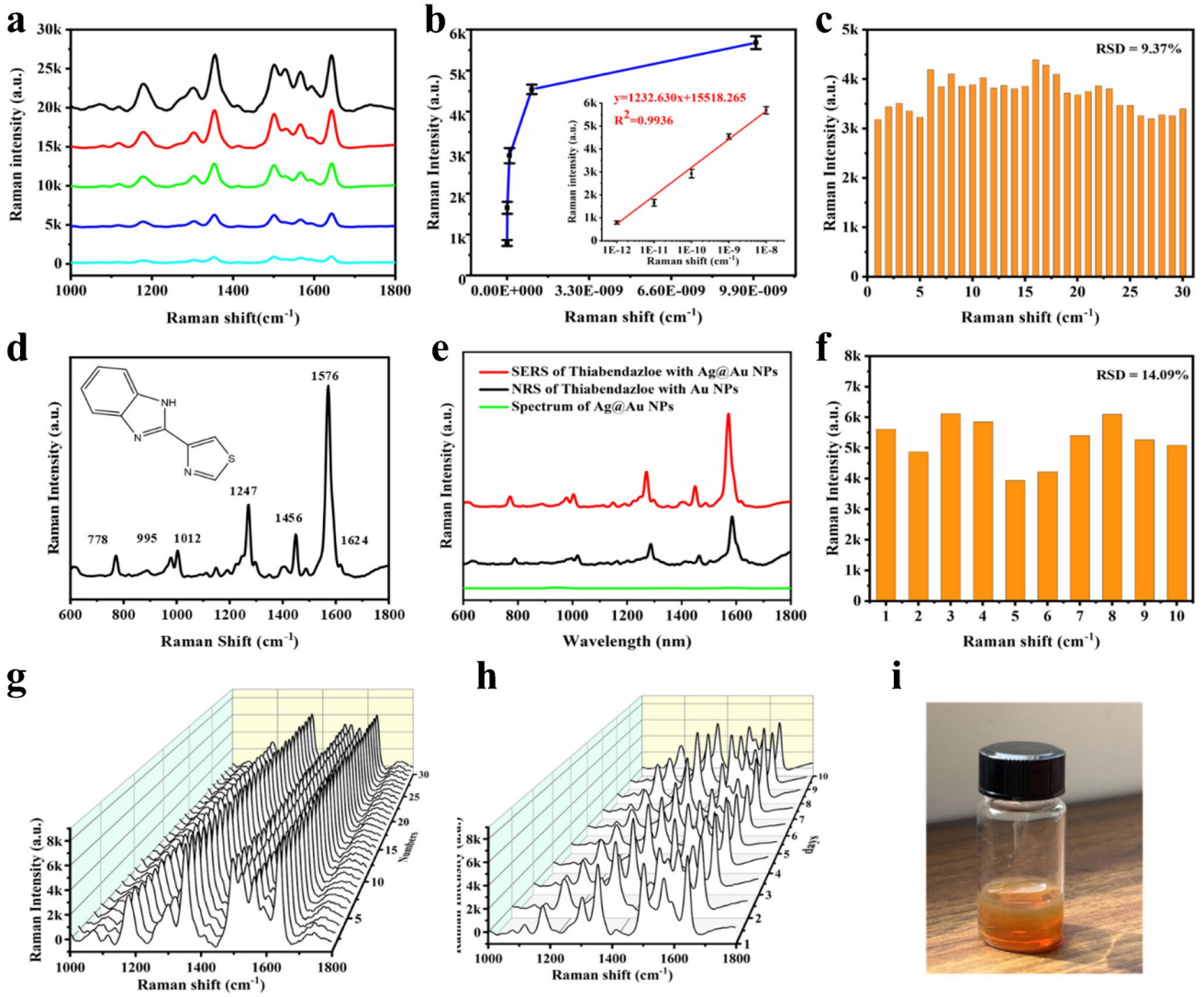

Fig. 5 SERS spectra of Au@Ag NPs adsorbed by different concentrations of R6G (**a**). The linear relationship between SERS intensity at 1654 cm^{-1} and the logarithm of different R6G concentration (**b**). **c** Repeated detection of the intensity distribution of SERS spectra at 1654 cm^{-1} for 30 same concentration of R6G, Raman spectrum of TBZ solid and its molecular structure picture (**d**). **e** Raman spectra of Au@Ag NPs and gold nanoparticles adsorbed by TBZ, respectively. **f** Intensity distribution of SERS spectra of R6G at 1645 cm^{-1} for 10 days of continuous testing, SERS spectra of 30 consecutive detections of the same concentration of R6G (**g**), SERS spectra of the same concentration of R6G for 10 consecutive days based on Au@Ag NPs after 20 days of storage (**h**), Au@Ag NPs solution after 10 days of storage at 4 °C (**i**)

after 10 days, the stored Au@Ag NPs solution remained well disseminated with neither agglomeration nor precipitation (Fig. 5i). The results show that the Au@Ag NPs solutions created in this study exhibit outstanding enhancing properties as well as good stability when stored for up to 20 days. As a result, the Au@Ag NPs may be useful in practical detection.

The analysis of TBZ characteristic peaks

On the as-synthesized Au@Ag NPs base, SERS spectra of a standard solution containing TBZ were obtained. Figure 5d depicts the molecular structure of TBZ as well as the solid's SERS spectrum. TBZ spectra show seven distinct peaks, which are 778, 995, 1012, 1247, 1456, 1576, and 1624 cm^{-1}, respectively. Table 1 shows the assignments

Table 1 Major special Raman peaks and band assignment of TBZ in the previous studies

Major special Raman peaks (cm^{-1})	Band assignment
778	C-S stretching, and bending of C=N bonds
995	Out of plane C-S-C, and C-H bending
1012	Stretching of C-N, and bending of N=C-N
1247	Stretching and deformation of C-H
1456	Bending and vibrations of C-H
1576 and 1624	Stretching of C=N bonds

of the SERS feature peaks. The faint Raman peak bands at 778, 995, 1012, and 1624 cm^{-1} are attributed to C-S stretching and bending of C=N bonds, out of plane C-S-C and C-H bending, stretching of C-N, and bending of N=C-N bonds. Other stronger peak bonds at 1247, 1456, and 1576 cm^{-1} could be connected with C-H stretching and deformation, C-H bending and vibrations, and C=N bond stretching [30–33]. Table 1 shows the vibrational modes that correlate to the character peaks.

The performance of the based-Au@Ag NPs sensor

The performance of the Raman spectra of 20 μg/mL TBZ combined with SERS of Au@Ag NPs and gold nanoparticles, respectively, and the Raman spectra of Au@Ag NPs on the Raman signal enhancement of TBZ molecules are compared in Fig. 5e to investigate the feasibility of Au@Ag NPs to improve Raman signals of TBZ molecules. The Au@Ag NPs exhibit no clear distinctive peaks, as seen in the picture, indicating that they do not affect SERS detection. Meanwhile, the SERS of TBZ had well-defined Raman peaks at 778, 995, 1012, 1247, 1456, 1576, and 1624 cm^{-1}, but it was clear that the enhancement was greater for Au@Ag NPs than for gold nanoparticles, because the enhancement of the electric field generated by laser excitation of the silver shell was far superior to that of gold. Furthermore, S bonds in TBZ molecules generate Ag-S bonds on the surface of Au@Ag NPs, resulting in TBZ molecules that are perpendicular to the nanoparticle surface. The SERS signal can be amplified to the greatest extent possible using the surface adsorption concept when the vibration mode of the absorbed

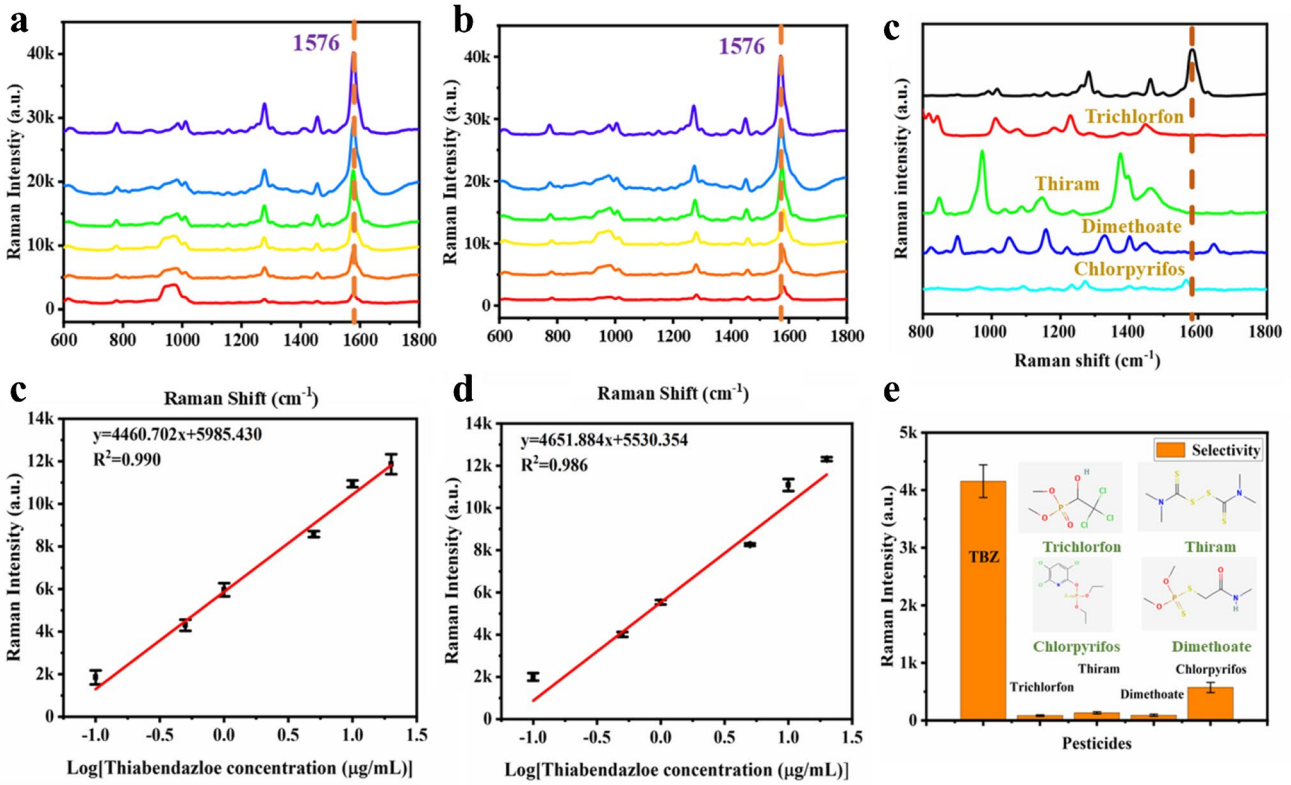

Fig. 6 SERS spectra of different concentrations of TBZ in standard solutions (**a**) and extracted real samples (**b**). Comparison of Raman spectra of pesticides TBZ, trichlorfon, thiram, dimethoate, and chlorpyrifos (**c**). The linear relationship between the SERS intensity of TBZ SERS spectra at 1576 cm^{-1} and the logarithmic concentration of TBZ combined in the standard solution and the actual samples, respectively (**d** and **e**). The selectivity of this proposed SERS sensor and molecular structure of trichlorfon, thiram, dimethoate, and chlorpyrifos (**f**)

Table 2 The result from SERS and ELISA for TBZ detection in spiked samples

Spiked concentration (μg/mL)	SERS			ELISA		
	Prediction value (μg/mL) (mean[a] ± SD[b])	RSD (%)	Recovery (%)	Detection value (μg/mL) (mean[a] ± SD[b])	RSD (%)	Recovery (%)
10	10.00 ± 0.69	6.92	100	10.30 ± 0.3	2.97	103
1	0.97 ± 0.05	4.98	96	1.09 ± 0.10	9.77	109
0.1	0.11 ± 0.01	8.63	105	0.10 ± 0.008	8.64	101

[a]Mean, the average value of six tests

[b]*SD*, standard deviation, $n = 6$

molecules is perpendicular to the absorbed metal surface [27]. This further reveals that Au@Ag NPs significantly increase TBZ molecules.

The quantitative analysis of TBZ in standard solution and apple juice samples

It is critical to use the newly designed SERS sensor for the quantitative detection of residue concentrations in food. Figure 6a shows the SERS spectra of varied concentrations of TBZ with Au@Ag NPs as the substrate to investigate the quantitative analytical performance of this sensor in standard solutions. As the concentration of TBZ falls, so does the SERS intensity of the TBZ characteristic peaks. The Raman characteristic peaks are also more apparent, even at 0.1 μg/mL concentration. The peak at 1576 cm^{-1} was selected to establish the SERS intensity as a function of TBZ concentration because it exhibited a greater and sharper SERS intensity than the other peaks. The usual quantitative analysis line between the SERS spectral intensity and the logarithm of concentration for the Raman characteristic peak of TBZ at 1576 cm^{-1} is shown in Fig. 6b. $y = 4460.702\ x + 5985.430$ is the fitted equation, with a coefficient of determination (R^2) of 0.990. This demonstrates that the SERS spectral signal of TBZ at concentrations ranging from 0.1 to 20 μg/mL has a strong linear relationship with concentration and may be utilized for quantitative prediction. The pesticide TBZ was identified in spiked apple juice to test the feasibility and usefulness of the suggested approach. Again, 2-μL droplets were applied dry on a clean silicon wafer for detection using a confocal Raman apparatus, and the qualitative and quantitative detection of the spiked pesticide TBZ was performed in less than 2 min. The characteristic peak of TBZ at 1576 cm^{-1} increased with TBZ concentration, and the linear relationship between the characteristic peak and concentration was similar to that of the standard solution (Fig. 6d and e), indicating that this method can be used for quantitative detection. Furthermore, using our suggested SERS sensor, the detection of TBZ attained a low concentration of 0.05 μg/mL in the actual sample, fulfilling the Chinese Department of TBZ minimal limit management.

Other pesticide interference experiments

In agriculture production, multiple pesticides are co-used to protect crops from pests and diseases. The simultaneous presence of multiple pesticides interferes with the detection of TBZ. To address this issue, anti-interference experiments were conducted in this study. The effects of other pesticide residues commonly found in fruit juices, such as trichlorfon, thiram, chlorpyrifos, and dimethoate, were studied (inset Fig. 6f). The results are shown in

Table 3 The comparison of previous studies and this proposed method for the detection of TBZ in food

Method	Tested sample	Testing equipment	Enhanced substrate	Data analysis	R^2	LOD	References
SERS	Rape	Portable Raman spectrometer	Ag NPs	PLS	0.94	0.1 ppm	[33]
SERS	Apple	Microscopy Raman spectrometer	Au NRs	Linear regression	0.977	0.1 ppm	[34]
SERS	Lemon	Confocal Raman spectrometer	Au@AgNRs/CMC/qPCR	Logarithmic fitting	0.9891	0.27 ppm	[35]
SERS	Apple	RK785-I Raman spectrometer	MoS_2/Au/Ag	Logarithmic fitting	0.988	0.1 ppm	[36]
SERS	Mango	Portable Raman spectrometer	Ag NFs	Regression fitting	0.98	0.24 ppm	[37]
This work	Apple	Confocal Raman spectrometer	Au@Ag NPs	Logarithmic fitting	0.986	0.05 ppm	This paper

Fig. 6c and f, where the SERS spectra of each of these interfering pesticides differ, due to the molecule-specific Raman spectral fingerprint information. At the same time, it can be observed that the interfering pesticides did not show obvious characteristic peaks at 1576 cm^{-1} and therefore had less effect on the quantitative detection of the pesticide TBZ. Furthermore, the strongest SERS signal was observed for TBZ, explaining the good enhancement effect and selectivity of the synthesized Au@Ag NPs.

Recovery analysis and comparison of the proposed method with other methods

The known SERS technique was used to assess the spiking recoveries of TBZ in apple juice. To detect TBZ, juice samples with concentrations of 10, 1, and 0.1 µg/mL were individually prepared and combined with Au@Ag NPs on clean silicon wafers. Six spectra were collected for each concentration. The acquired SERS spectra were then analyzed using a previously developed SERS algorithm for content prediction. Table 2 presents the calculated predicted values and recoveries of the samples using this method and the enzyme-linked immunosorbent assay (ELISA) as a comparison. The recoveries for the three TBZ concentrations in the samples ranged from 96 to 105% for SERS and 101 to 109% for ELISA, with no significant differences observed in the relative standard deviations (RSD) between the two methods. These findings demonstrate that the proposed approach can effectively quantify TBZ in apple samples.

In addition, the appropriate Au@Ag NPs created so far were compared with other SERS previously explored for the detection of TBZ in fruits, and the findings are shown in Table 3. It is worth noting that the core-shell size nanoparticle paired with the SERS approach proposed in this research has high sensitivity in the evaluation of pesticide residues. Moreover, these nanoparticles offer the advantage of being cost-effective and easy to prepare, further enhancing their practical applicability.

Conclusions

In this study, Au@Ag NPs with variable shell thickness were synthesized and utilized as SERS-enhanced substrates for the quantitative detection of TBZ in apple juice. Different thicknesses of Au@Ag NPs in colors ranging from burgundy to orange were effectively produced and analyzed using UV-Vis spectroscopy, TEM images, and HAADF-STEM. The findings revealed that the Au@Ag NPs have bimetallic gold and silver characteristics. The findings indicated that Au@Ag NPs with a silver shell thickness of 7.3 nm and bimetallic gold and silver characteristics were chosen as the best-enhancing substrate, and the SERS spectrum of R6G was well identified in the 10^{-5} M to 10^{-12} M range. The TBZ feature peak at 1576 cm^{-1} was chosen for further investigation of the link between Raman intensity and concentration. The current study used a simple approach and effectively detected TBZ in apple samples with a high R^2 of 0.986, while the recovery analysis and RSD were within a tolerable range. Furthermore, the LOD for 0.05 µg/mL TBZ was found in genuine samples. These findings show that the developed SERS method was used to rapidly detect TBZ in apple juices. The applicability of our proposed method for the detection of other pesticides or contaminants in food needs to be further explored. Additionally, we target to further optimize and analyze the synthesis technique of the SERS substrate to improve the sensitivity and accuracy of the detection.

Supplementary Information The online version contains supplementary material available at https://doi.org/10.1007/s00216-023-05055-1.

Acknowledgements The authors are thankful to the Henan Provincial Science and Technology Research Project (GZS2021007) and the National Natural Science Foundation of China (grant number 32071890, 31671581).

Author contribution Conceptualization: Xiaodong Li. Methodology: Xiaodong Li. Writing—original draft preparation: Xiaodong Li, Yanyan Zhang, Muhammad Awais. Writing—review and editing: Xiaodong Li, Syed Muhammad Zaigham Abbas Naqvi, Linze Li, Hao Zhang, Yani Xiong. Project administration: Jiandong Hu. All authors have read and agreed to the published version of the manuscript.

Declarations

Conflict of interest The authors declare no competing interests.

References

1. Wang W, Wan Q, Li Y, Xu W, Yu X. Uptake, translocation and subcellular distribution of pesticides in Chinese cabbage (Brassica rapa var. chinensis). Ecotox Environ Safe. 2019;183. https://doi.org/10.1016/j.ecoenv.2019.109488.
2. Yan X, Li H, Su X. Review of optical sensors for pesticides. Trac-Trend Anal Chem. 2018;103:1–20. https://doi.org/10.1016/j.trac.2018.03.004.
3. Farkhondeh T, Mehrpour O, Forouzanfar F, Roshanravan B, Samarghandian S. Oxidative stress and mitochondrial dysfunction in organophosphate pesticide-induced neurotoxicity and its amelioration: a review. Environ Sci Pollut R. 2020;27(20):24799–814. https://doi.org/10.1007/s11356-020-09045-z.
4. Ruengprapavut S, Sophonnithiprasert T, Pongpoungphet N. The effectiveness of chemical solutions on the removal of carbaryl residues from cucumber and chili presoaked in carbaryl using the HPLC technique. Food Chem. 2020;309. https://doi.org/10.1016/j.foodchem.2019.125659.
5. Saito-Shida S, Kashiwabara N, Nemoto S, Akiyama H. Development of an LC-MS/MS-based method for determination of acetochlor and its metabolites in crops. J Food Compos Anal. 2022;108. https://doi.org/10.1016/j.jfca.2022.104454.

6. Zhao YL, Hou XA, Qin DM, Liu D. Dispersive liquid-liquid microextraction method for the simultaneous determination of four isomers of hexachlorocyclohexane and six pyrethroid pesticides in milk by gas chromatography electron capture detector. Food Anal Method. 2020;13(2):370–81. https://doi.org/10.1007/s12161-019-01662-w.
7. Munoz R, Guevara-Lara A, Santos JLM, Miranda JM, Rodriguez JA. Determination of glyphosate in soil samples using CdTe/CdS quantum dots in capillary electrophoresis. Microchem J. 2019;146:582–7. https://doi.org/10.1016/j.microc.2019.01.059.
8. Han C, Hu B, Huang C, Zhang W, Wu H, Liu C, et al. Determination of morpholine residue in fruit and fruit juices by gas chromatography-tandem mass spectrometry. Lwt-Food Sci Technol. 2022;161. https://doi.org/10.1016/j.lwt.2022.113369.
9. Xue YC, Zhu CY, Jiang H. Comparison of the performance of different one-dimensional convolutional neural network models-based near-infrared spectra for determination of chlorpyrifos residues in corn oil. Infrared Phys Techn. 2023;132. https://doi.org/10.1016/j.infrared.2023.104734.
10. Mishra A, Kukreja EA, Pudake RN, Kumar R, Singh MP, Yadav L, et al. Label-free selective and sensitive colorimetric detection of ampicillin in milk and water using silver nanoparticles. J Food Compos Anal. 2023;119. https://doi.org/10.1016/j.jfca.2023.105256.
11. Chafiqi N, Karamoko G, Chene C, Pelzer E, Vanderriele M, Karoui R, et al. Development of 2D and 3D front face fluorescence spectroscopy for monitoring ultrasound treatment in the removal of pesticides residues from fresh lettuces at the laboratory and pilot scales. Spectrochim Acta A. 2023;290:1386–425. https://doi.org/10.1016/j.saa.2022.122278.
12. Ou Q, Tang B, Jiang L, Han M, Yang W, Tang J, et al. Quantitative determination of carbosulfan residues by surface-enhanced Raman spectroscopy. Spectrochim Acta A.. 2023;290. https://doi.org/10.1016/j.saa.2022.122315.
13. Umapathi R, Park B, Sonwal S, Rani GM, Cho YJ, Huh YS. Advances in optical-sensing strategies for the on-site detection of pesticides in agricultural foods. Trends Food Sci Tech. 2022;119:69–89. https://doi.org/10.1016/j.tifs.2021.11.018.
14. Lin S, Fang XY, Fang GQ, Liu FP, Dong HY, Zhao HY, et al. Ultrasensitive detection and distinction of pollutants based on SERS assisted by machine learning algorithms. Sensor Actuat B-Chem. 2023;384. https://doi.org/10.1016/j.snb.2023.133651.
15. Wang KQ, Sun DW, Pu HB, Wei QY. Surface-enhanced Raman scattering of core-shell Au@Ag nanoparticles aggregates for rapid detection of difenoconazole in grapes. Talanta. 2019;191:449–56. https://doi.org/10.1016/j.talanta.2018.08.005.
16. Du X, Gao Z, Yang T, Qu Y, He L. Understanding the impact of a non-ionic surfactant alkylphenol ethoxylate on surface-enhanced Raman spectroscopic analysis of pesticides on apple surfaces. Spectrochim Acta A. 2023;301. https://doi.org/10.1016/j.saa.2023.122954.
17. Xu Y, Gu F, Hu S, Wu Y, Wu C, Deng Y, et al. A cell wall-targeted organic-inorganic hybrid nano-catcher for ultrafast capture and SERS detection of invasive fungi. Biosens Bioelectron. 2023;228. https://doi.org/10.1016/j.bios.2023.115173.
18. Huang Y-H, Wei H, Santiago PJ, Thrift WJ, Ragan R, Jiang S. Sensing antibiotics in wastewater using surface-enhanced Raman scattering. Environ Sci Technol. 2023;57(12):4880–91. https://doi.org/10.1021/acs.est.3c00027.
19. Kim K, Han DK, Choi N, Kim SH, Joung Y, Kim K, et al. Surface-enhanced Raman scattering-based dual-flow lateral flow assay sensor for the ultrasensitive detection of the thyroid-stimulating hormone. Anal Chem. 2021;93(17):6673–81. https://doi.org/10.1021/acs.analchem.0c05336.
20. Yu Q, Trinh HD, Lee Y, Kang T, Chen L, Yoon S, et al. SERS-ELISA using silica-encapsulated Au core-satellite nanotags for sensitive detection of SARS-CoV-2. Sensor Actuat B-Chem. 2023;382. https://doi.org/10.1016/j.snb.2023.133521.
21. Wang T, Wang S, Cheng Z, Wei J, Yang L, Zhong Z, et al. Emerging core–shell nanostructures for surface-enhanced Raman scattering (SERS) detection of pesticide residues. Chem Eng J. 2021;424. https://doi.org/10.1016/j.cej.2021.130323.
22. Wang KQ, Sun DW, Pu HB, Wei QY. Shell thickness-dependent Au@Ag nanoparticles aggregates for high-performance SERS applications. Talanta. 2019;195:506–15. https://doi.org/10.1016/j.talanta.2018.11.057.
23. Oliveira MJS, Rubira RJG, Furini LN, Batagin-Neto A, Constantino CJL. Detection of thiabendazole fungicide/parasiticide by SERS: quantitative analysis and adsorption mechanism. Appl Surf Sci. 2020;517. https://doi.org/10.1016/j.apsusc.2020.145786.
24. National food safety standard–Maximum residue limits for pesticides in food. Standardization administration of the People's Republic of China. GB 2021;2763–21.
25. Lin L, Wu R-m, Liu M-h, Wang X-b, Yan L-y. Surface-enhanced Raman spectroscopy analysis of thiabendazole pesticide. Spectrosc Spect Anal. 2015;35(2):404–8. https://doi.org/10.3964/j.issn.1000-0593(2015)02-0404-05.
26. Hussain N, Pu H, Sun DW. Synthesis of bimetallic core-shelled nanoparticles modified by 2-mercaptoethanol as SERS substrates for detecting ferbam and thiabendazole in apple puree. Food Addit Contam A. 2021;38(8):1386–99. https://doi.org/10.1080/19440049.2021.1933207.
27. Chen ZY, Sun Y, Shi JY, Zhang W, Zhang XA, Huang XW, et al. Facile synthesis of Au@Ag core-shell nanorod with bimetallic synergistic effect for SERS detection of thiabendazole in fruit juice. Food Chem. 2022;370. https://doi.org/10.1016/j.foodchem.2021.131276.
28. Zhang Y, Zhang H, Li D, Abbas Naqvi SMZ, Abdulraheem MI, Su R, et al. Surface-enhanced Raman spectroscopy for the quantitative detection of abscisic acid in wheat leaves using silver coated gold nanocomposites. Spectrosc Lett. 2021;54(10):732–41. https://doi.org/10.1080/00387010.2021.1995439.
29. Liou P, Nayigiziki FX, Kong F, Mustapha A, Lin M. Cellulose nanofibers coated with silver nanoparticles as a SERS platform for detection of pesticides in apples. Carbohyd Polym. 2017;157:643–50. https://doi.org/10.1016/j.carbpol.2016.10.031.
30. Teixeira CA, Poppi RJ. Paper-based SERS substrate and one-class classifier to monitor thiabendazole residual levels in extracts of mango peels. Spectrochim Acta A. 2020;229. https://doi.org/10.1016/j.saa.2019.117913.
31. Alsammarraie FK, Lin M, Mustapha A, Lin H, Chen X, Chen Y, et al. Rapid determination of thiabendazole in juice by SERS coupled with novel gold nanosubstrates. Food Chem. 2018;259:219–25. https://doi.org/10.1016/j.foodchem.2018.03.105.
32. Hussain A, Pu HB, Hu BX, Sun DW. Au@Ag-TGANPs based SERS for facile screening of thiabendazole and ferbam in liquid milk. Spectrochim Acta A. 2021;245. https://doi.org/10.1016/j.saa.2020.118908.
33. Fu GD, Sun DW, Pu HB, Wei QY. Fabrication of gold nanorods for SERS detection of thiabendazole in apple. Talanta. 2019;195:841–9. https://doi.org/10.1016/j.talanta.2018.11.114.
34. Lin L, Dong T, Nie PC, Qu FF, He Y, Chu BQ, et al. Rapid determination of thiabendazole pesticides in rape by surface enhanced Raman spectroscopy. Sensors-Basel. 2018;18(4). https://doi.org/10.3390/s18041082.
35. Hu BX, Pu HB, Sun DW. Flexible Au@AgNRs/CMC/qPCR film with enhanced sensitivity, homogeneity and stability for in-situ extraction and SERS detection of thiabendazole on fruits. Food

Chem. 2023;423. https://doi.org/10.1016/j.foodchem.2023.135840.
36. Yu XX, Sun Y, Hu JY, Wang JJ, Zhuang XM, Zhang SH, et al. MoS2/Au/Ag nanostructures for ratiometric surface-enhanced Raman scattering determination of pesticide residues. Acs Appl Nano Mater. 2023;6(1):685–94. https://doi.org/10.1021/acsanm.2c04843.
37. Li HH, Luo XF, Haruna SA, Zhou WJ, Chen QS. Rapid detection of thiabendazole in food using SERS coupled with flower-like AgNPs and PSL-based variable selection algorithms. J Food Compos Anal. 2023;115. https://doi.org/10.1016/j.jfca.2022.105016.